Infrared Spectra of $RhCO^+$, RhCO, and $RhCO^-$ in Solid Neon: A Scale for Charge in Supported Rh(CO) Catalyst Systems

Mingfei Zhou and Lester Andrews*

Contribution from the Department of Chemistry, University of Virginia, Charlottesville, Virginia 22901

Received April 14, 1999

Abstract: Laser-ablated Rh^+, Rh, and electrons react with CO on condensation in excess neon at 4 K to form $RhCO^+$, RhCO, $RhCO^-$, and $Rh(CO)_2^+$, $Rh(CO)_2$, $Rh(CO)_2^-$, and higher carbonyls. These rhodium carbonyls are identified by isotopic substitution (^{13}CO, $C^{18}O$, and mixtures), electron trapping with added CCl_4, and comparison with DFT calculations of isotopic frequencies. This is the first spectroscopy of isolated rhodium carbonyl cations and anions. The isolated monocarbonyl species provide a scale to estimate local charge on Rh(CO) sites in catalyst systems.

Introduction

Rhodium-supported catalyst systems are used for many important reactions including hydrogenation of carbon monoxide, the reduction of nitric oxide in automobile exhaust gas, and the hydroformylation of olefins. The chemisorption of CO on supported Rh produces a discrete $Rh(CO)_2$ species, and the oxidation state and charge on the metal center have been considered.[1−9] This gem−rhodium dicarbonyl species is usually designated $Rh^I(CO)_2$ because of agreement with the C−O stretching modes of the $(OC)_2Rh(Cl)_2Rh(CO)_2$ molecule, where the oxidation state of rhodium is +1.[6,7,9] The rhodium dicarbonyl on alumina, silica, and zeolites is widely used as a catalyst system for activation of many molecules including H_2, N_2, CO_2, and alkanes[10−15] through a coordinatively unsaturated $Rh^I(CO)$ center, which absorbs near 2096 cm^{-1} on zeolites,[16] 2070 cm^{-1} on silica,[17] and 2060 cm^{-1} on alumina.[4,11] Furthermore, the activation of C−H bonds in alkanes by a transient CpRh(CO) species absorbing near 1985 cm^{-1} in the gas phase readily occurs.[18,19] In addition, the rhodium−phosphine complexes, $Rh(CO)(Cl)(PR_3)_2$, exhibit carbonyl frequencies ranging from 2016 cm^{-1} (R = OPh) to 1956 cm^{-1} (R = Et).[20] What is the local charge on the Rh(CO) centers in these active species?

Linearly adsorbed CO on Rh(100) at 90 K for 0.1 monolayer coverage gives a 2013 cm^{-1} carbonyl band.[21] The absorption for RhCO in solid neon at 2022 cm^{-1} just observed in our laboratory is near this metal surface absorption and provides a measure of the isolated neutral RhCO molecule vibrational frequency. Clearly the above active catalyst Rh(CO) species have both higher and lower C−O stretching fundamentals. We suggest the carbonyl frequencies of the $RhCO^+$, RhCO, and $RhCO^-$ series isolated in solid neon as a scale for determining local charge on the metal carbonyl. The calculated Mulliken charge distributions on these species show an increase in electron density in the CO π^* orbital, which *decreases* the C−O frequency. We report here neon matrix spectra of $RhCO^+$, RhCO, $RhCO^-$ and of $Rh(CO)_2^+$, $Rh(CO)_2$, $Rh(CO)_2^-$ as models for local charge in active catalyst species.

A variety of theoretical calculations have been performed on rhodium carbonyl species using different levels of theory and basis sets.[22−26] Vibrational frequencies clearly depend on the methods employed. We have found that density functional theory (DFT) using the Becke−Perdue functional, modest basis sets, and effective core potentials predict first row transition metal[27−30] and ruthenium[31] carbonyl cation, neutral and anion

(1) Yang, A. C.; Garland, C. W. *J. Phys. Chem.* **1957**, *61*, 1504.
(2) Garland, C. W.; Lord, R. C.; Troiano, P. F. *J. Phys. Chem.* **1965**, *69*, 1188.
(3) Yates, J. T., Jr.; Duncan, T. M.; Worley, S. D.; Vaughn, R. W. *J. Chem. Phys.* **1979**, *70*, 1219.
(4) Cavanagh, R. R.; Yates, J. T., Jr. *J. Chem. Phys.* **1981**, *74*, 4150.
(5) Rice, C. A.; Worley, S. D.; Curtis, C. W.; Guin, J. A.; Tanner, A. R. *J. Chem. Phys.* **1981**, *74*, 6487.
(6) Yates, J. T., Jr.; Kolasinski, K. *J. Chem. Phys.* **1983**, *79*, 1026. Paul, D. P.; Ballinger. T. H.; Yates, J. T. ,Jr. *J. Phys. Chem.* **1990**, *94*, 4617.
(7) van't Blik, H. F. J.; van Zon, J. B. A. D.; Huizinga, T.; Vis, J. C.; Koningsberger, D. C.; Prins, R. *J. Am. Chem. Soc.* **1985**, *107*, 3139.
(8) Robbins, J. L. *J. Phys. Chem.* **1986**, *90*, 3381.
(9) Wovchko, E. A.; Zubkov, T. S.; Yates, J. T., Jr. *J. Phys. Chem. B* **1998**, *102*, 10535. Zubkov, T. S.; Wovchko, E. A.; Yates, J. T., Jr. *J. Phys. Chem.*, in press.
(10) Wovchko, E. A.; Yates, J. T., Jr. *J. Am. Chem. Soc.* **1995**, *117*, 12577.
(11) Wovchko, E. A.; Yates, J. T., Jr. *J. Am. Chem. Soc.* **1996**, *118*, 10250.
(12) Wovchko, E. A.; Yates, J. T., Jr. *J. Am. Chem. Soc.* **1998**, *120*, 7544.
(13) Fisher, I. A.; Bell, A. T. *J. Catalysis* **1996**, *162*, 54.
(14) Ballinger, T. H.; Yates, J. T., Jr. *J. Am. Chem. Soc.* **1992**, *114*, 10074.
(15) Erdöhelyi, A.; Cserényi, J.; Solyumosi, F. *J. Catal.* **1993**, *141*, 287.
(16) Miessner, H. *J. Am. Chem. Soc.* **1994**, *116*, 11522.
(17) Anderson, J. A.; Rochester, C. H.; Wang, Z. J. *J. Mol. Catal. A* **1999**, *139*, 285.
(18) Wasserman, E. P.; Moore, C. B.; Bergman, R. G. *Science* **1992**, *255*, 315.
(19) Bengali, A. A.; Schultz, R. H.; Moore, C. B.; Bergman, R. G. *J. Am. Chem. Soc.* **1994**, *116*, 9585.
(20) Serron, S.; Nolan, S. P.; Moloy, K. G. *Organometallics* **1996**, *15*, 4301 and references therein.
(21) Leung, L.-W.; He, J.-W.; Goodman, D. W. *J. Chem. Phys.* **1990**, *93*, 8328.
(22) McKee, M. L.; Worley, S. D. *J. Phys. Chem.* **1988**, *92*, 3699; *J. Phys. Chem. A* **1997**, *101*, 5600.
(23) Barnes, L. A.; Rosi, M.; Bauschlicher, C. W. Jr. *J. Chem. Phys.* **1990**, *93*, 609.
(24) Mains, G. J.; White, J. M. *J. Phys. Chem.* **1991**, *95*, 112.
(25) Papai, I.; Goursot, A.; St. Amant, A.; Salahub D. R. *Theor. Chim. Acta* **1992**, *84*, 217.
(26) Dai, D.; Balasubramanian, K. *J. Chem. Phys.* **1994**, *101*, 2148.
(27) Zhou, M. F.; Andrews, L. *J. Chem. Phys.* **1999**, *110*, 10370.
(28) Zhou, M. F.; Andrews, L. *J. Phys. Chem. A* **1999**, *103*, 2964.
(29) Zhou, M. F.; Andrews, L. *J. Phys. Chem. A*, **1999**, *103*, 5259.
(30) Zhou, M. F.; Andrews, L. *J. Chem. Phys.* **1999**, *111*, 4548.
(31) Zhou, M. F.; Andrews, L. *J. Phys. Chem. A* **1999**, *103*, 6956.

10.1021/ja991180j CCC: $18.00
Published on Web 09/21/1999

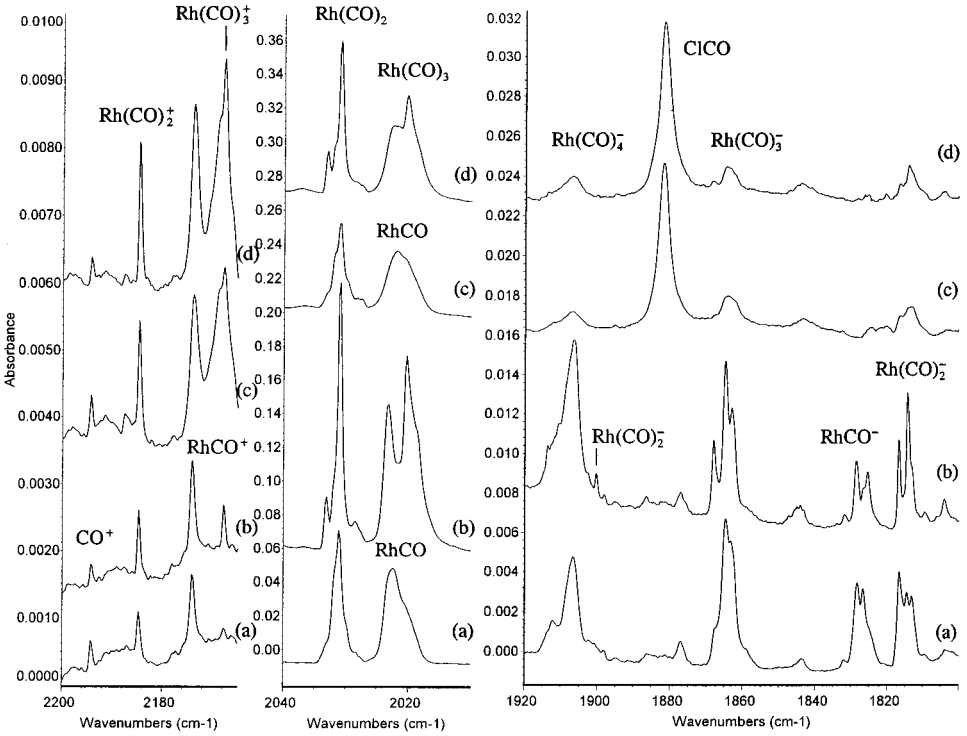

Figure 1. Infrared spectra in the 2200−2165 cm^{-1}, 2040−2010 cm^{-1}, and 1920−1800 cm^{-1} regions for laser-ablated rhodium and 0.2% CO in neon at 4 K after (a) sample codeposition for 30 min, (b) annealing to 8 K, (c) 0.01% CCl_4 and 0.2% CO sample codeposition for 30 min, and (d) annealing to 8 K. Note different absorbance scales.

frequencies in solid neon *within 1−2%*. Accordingly, we report here analogous DFT calculations on Rh carbonyl cation, neutral, and anion complexes. In addition, we calculate a complete set of $^{12}C^{16}O$, $^{13}C^{16}O$, and $^{12}C^{18}O$ isotopic frequencies to compare with observed values to characterize normal vibrational modes for these carbonyl species.

Experimental and Computational Methods

The experiment for laser ablation and matrix isolation spectroscopy has been described in detail previously.[32−35] Briefly, the Nd:YAG laser fundamental (1064 nm, 10 Hz repetition rate, 10ns pulse width) was focused on the rotating rhodium target using low energy (1−5 mJ/pulse), and rhodium atoms, cations, and electrons were codeposited with carbon monoxide (0.2%) in neon onto a 4 K CsI cryogenic window at 2−4 mmol/h.

Density functional theory (DFT) calculations were done to support band identifications using the Gaussian 94 program, the BP86 functional, the D95* basis sets for C and O atoms, and Los Alamos ECP plus DZ basis set for metal atoms.[38−41]

Results and Discussion

Infrared Spectra and Calculations. A representative spectrum is shown in Figure 1a with the effect of annealing to 8 K in Figure 1b. Strong CO absorption and weak CO^+, $(CO)_2^+$, and $(CO)_2^-$ absorptions[27,28,36] are observed. An identical experiment with 0.01% CCl_4 added is illustrated in scans (c) and (d). Clearly, bands in the 2200−2165 cm^{-1} region are enhanced by CCl_4, products in the 2040−2010 cm^{-1} region are little affected, but bands in the 1920−1800 cm^{-1} region are markedly decreased. Experiments were also done with ^{13}CO, $C^{18}O$, and a mixture of ^{12}CO and ^{13}CO, and the product absorptions are listed in Table 1. Calculations were performed on the monocarbonyl and dicarbonyl neutrals, cations and anions, and the isotopic carbonyl frequencies are listed in Tables 2 and 3 for comparison with experiment.

Rhodium Carbonyl Assignments. The two strongest bands at 2031.0 and 2022.5 cm^{-1} with Rh and CO in neon increase on annealing and acquire site splittings at 2033.2 and 2023.5 cm^{-1} (Figure 1). In the ^{13}CO sample, these bands shift to 1986.8 and 1975.1 cm^{-1}. Mixed $^{12}CO + {}^{13}CO$ isotopic spectra show the same two broader bands as a doublet at 2022.5 and 1975.1 cm^{-1} identifying the vibration of a single carbonyl and show three sharp absorptions forming a 2031.0, 2003.2, 1986.8 cm^{-1} triplet with a *new* intermediate component characterizing the vibration of two equivalent carbonyl submolecules. The 2022.5 and 2031.0 cm^{-1} bands are assigned to RhCO and the antisymmetric C−O stretching mode of $Rh(CO)_2$, respectively, in agreement with the argon matrix bands (2008.0 and 2012.8 cm^{-1}) from thermal Rh atom reactions.[42]

These assignments are confirmed by DFT calculations. Although the $^2\Sigma^+$ state is calculated to be slightly lower than

(32) Burkholder, T. R.; Andrews, L *J. Chem. Phys.* **1991**, *95*, 8697; Hassanzadeh, P.; Andrews, L. *J. Phys. Chem.* **1992**, *96*, 9177.
(33) Zhou, M. F.; Andrews, L. *J. Am. Chem. Soc.* **1998**, *120*, 11499.
(34) Zhou, M. F.; Chertihin, G. V.; Andrews, L. *J. Chem. Phys.* **1998**, *109*, 10893.
(35) Zhou, M. F.; Andrews, L. *J. Phys Chem. A* **1998**, *102*,10250. The $CoCO^-$ state is $^3\Delta$.
(36) Thompson, W. E.; Jacox, M. E. *J. Chem. Phys.* **1991**, *95*, 735.
(37) The 1881.9 cm^{-1} band is due to the C−O stretch of ClCO, which has been observed at 1877.0 cm^{-1} in solid argon; see: Jacox, M. E.; Milligan, D. E. *J. Chem. Phys.* **1965**, *43*, 866.
(38) Frisch, M. J.; Trucks, G. W.; Schlegel, H. B.; Gill, P. M. W.; Johnson, B. G.; Robb, M. A.; Cheeseman, J. R.; Keith, T.; Petersson, G. A.; Montgomery, J. A.; Raghavachari, K.; Al-Laham, M. A.; Zakrzewski, V. G.; Ortiz, J. V.; Foresman, J. B.; Cioslowski, J.; Stefanov, B. B.; Nanayakkara, A.; Challacombe, M.; Peng, C. Y.; Ayala, P. Y.; Chen, W.; Wong, M. W.; Andres, J. L.; Replogle, E. S.; Gomperts, R.; Martin, R. L.; Fox, D. J.; Binkley, J. S.; Defrees, D. J.; Baker, J.; Stewart, J. P.; Head-Gordon, M.; Gonzalez, C.; Pople, J. A. *Gaussian 94, Revision B.1*; Gaussian, Inc.: Pittsburgh, PA, 1995.
(39) Perdew, J. P. *Phys. Rev. B* **1986**, *33*, 8822; Becke, A. D. *J. Chem. Phys.* **1993**, *98*, 5648.
(40) Dunning, T. H., Jr.; Hay, P. J. *Modern Theoretical Chemistry*; Schaefer, H. F., III, Ed.; Plenum: NewYork, 1976.
(41) Hay, P. J.; Wadt, W. R. *J. Chem. Phys.* **1985**, *82*, 299.
(42) Ozin, G. A.; Hanlan, A. J. L. *Inorg. Chem.* **1979**, *18*, 2091.

Table 1. Infrared Absorptions (cm^{-1}) from Codeposition of Laser-Ablated Rh Atoms, Cations, and Electrons with CO in Excess Neon at 4 K

$^{12}C^{16}O$	$^{13}C^{16}O$	$^{12}C^{18}O$	$^{12}C^{16}O + {}^{13}C^{16}O$	*R*(12/13)	*R*(16/18)	assignment
2194.3	2145.8			1.0226		CO^+
2184.7	2136.3	2133.1		1.0227	1.0242	$Rh(CO)_2^+$
2174.1	2125.0	2123.8		1.0231	1.0237	$RhCO^+$
2167.8	2119.9	2116.4		1.0226	1.0243	$Rh(CO)_3^+$
2160.1	2112.4	2108.9	2160.1, 2112.4	1.0226	1.0243	$(CO)_x$
2140.7	2093.6	2089.7	2140.7, 2093.6	1.0225	1.0244	CO
2056.3	2010.9	2007.4	2056.3, 2018.4, 2010.9	1.0226	1.0244	$(CO)_2^+$
2033.2	1989.0	1984.4	2108.0, 2033.4, 2005.5, 1989.1	1.0222	1.0246	$Rh(CO)_2$ site
2031.0	1986.8	1982.2	2105.0, 2031.0, 2003.2, 1986.8	1.0222	1.0246	$Rh(CO)_2$
2023.5	1976.0	1979.6	2023.5, 1976.0	1.0240	1.0218	RhCO site
2022.5	1975.1	1979.3	2022.5, 1974.9	1.0240	1.0218	RhCO
2020.3	1976.0	1972.2	2020.4, 2010.3, 1995.3, 1989.1, 1976.0	1.0224	1.0244	$Rh(CO)_3$
2018.5	1974.3	1970.7		1.0224	1.0243	$Rh(CO)_4$
1906.4	1863.0	1863.6	1906.4, 1891.1, 1880.5, 1870.3, 1862.8	1.0233	1.0230	$Rh(CO)_4^-$
1902.7	1856.6			1.0248		$Rh(CO)_2^-$
1900.4	1854.7		1900.4, 1882.7, 1854.7	1.0246		$Rh(CO)_2^-$
1864.8	1822.4	1822.5	1864.8, 1845.3, 1833.0, 1822.4	1.0233	1.0232	$Rh(CO)_3^-$
1862.8	1820.6	1820.9	1862.8, 1843.5, 1830.8, 1820.5	1.0232	1.0231	$Rh(CO)_3^-$
1828.6	1782.7	1793.7	1828.4, 1782.7	1.0257	1.0195	$RhCO^-$
1826.7	1781.2	1791.9	1826.6, 1781.2	1.0255	1.0194	$RhCO^-$ site
1825.8	1783.4	1785.3		1.0238	1.0227	Rh_xCO
1816.7	1774.8	1776.6	1816.6, 1790.2, 1774.8	1.0236	1.0226	$Rh(CO)_2^-$
1814.4	1772.6	1774.2	1814.5, 1788.2, 1772.7	1.0236	1.0227	$Rh(CO)_2^-$
1517.4	1484.2	1481.2	1517.4, 1499.4, 1484.2	1.0224	1.0244	$(CO)_2^-$

Table 2. Bond Lengths, Isotopic C−O Stretching Frequencies (cm^{-1}), Intensities (km/mol), and Isotopic Frequency Ratios Calculated for Rhodium Monocarbonyl States

molecule	BL(Å)[a]	$^{12}C^{16}O$	$^{13}C^{16}O$	$^{12}C^{18}O$	*R*(12/13)	*R*(16/18)
$RhCO^+(^3\Delta)$[b]	1.903,	2129.4	2079.9	2081.1	1.0238	1.0232
	1.152	(238)	(223)	(234)		
$RhCO\ (^2\Delta)$[b]	1.822,	2004.7	1955.8	1962.6	1.0250	1.0215
	1.777	(504)	(47)	(487)		
$RhCO\ (^2\Sigma^+)$[b]	1.789,	1962.8	1914.8	1921.9	1.0251	1.0213
	1.184	(486)	(461)	(469)		
$RhCO^-\ (^1\Sigma^+)$[b]	1.736,	1843.6	1795.5	1810.0	1.0268	1.0186
	1.212	(757)	(725)	(719)		

[a] Rh−C, C−O. [b] Relative energies (kcal/mol): $^2\Delta$ (0.0), $^2\Sigma^+$ (−0.8), $^1\Sigma^+$ (−34.5), $^3\Delta$ (+193.3).

$^2\Delta$ at the BP86 level, earlier ab initio and B3LYP calculations, which determine energies more accurately, found the $^2\Delta$ state to be lower.[22,26] Furthermore, the frequency match is much better for the $^2\Delta$ state. The isotopic $^{12}CO/^{13}CO$ and $C^{16}O/C^{18}O$ frequency ratios are the same for both states, which are very close to the observed ratios for RhCO (Table 2). Our BP86 calculations predict four low energy $Rh(CO)_2$ states, but the $^2\Delta_g$ state antisymmetric C−O stretching mode calculated at 2004.1 cm^{-1} fits the 2031.0 cm^{-1} observed value better (Table 3). The linear structure is confirmed by observation of a weak symmetric stretching mode only for the $Rh(^{12}CO)(^{13}CO)$ isotopic molecule (2105.0 cm^{-1}). The B3LYP functional, which determines more accurate energies, finds $^2\Delta_g$ to be the ground state of the isolated molecule. These calculations show that bent and linear $Rh(CO)_2$ states have nearly the same energy, and even though the linear $^2\Delta_g$ state characterized here in solid neon is apparently the lowest state, the $Rh(CO)_2$ radical can be bent easily in other environments (to form another bond to Rh). The scale factors (observed/calculated) for RhCO and $Rh(CO)_2$, 1.009 and 1.013, are appropriate for this level of theory,[43] i.e., the predictions are 0.9 and 1.3% lower than observed values.

The 2020.3 cm^{-1} absorption that grows markedly on annealing is assigned to $Rh(CO)_3$. Mixed isotopic spectra show three intermediate components, which is consistent with the C_{2v} (T-shaped) structure calculated by DFT.[44] The strongest mode is predicted at 1981.4 cm^{-1} just 1.9% below the observed value. In addition, the 2018.5 cm^{-1} shoulder increases on annealing and is assigned to $Rh(CO)_4$ in agreement with the previous thermal Rh atom work, which conclusively identified $Rh(CO)_4$ at 2010 cm^{-1} in solid argon.[42]

The 1816.7, 1828.6, 1864.8, and 1906.4 cm^{-1} bands are due to carbonyl vibrations of the $Rh(CO)_x^-$ anions. These bands *decreased* to less than 10% of their absorbance when the sample was doped with CCl_4, which preferentially traps electrons and supports the anion identification.[27,30,33−35] First, the 1828.6 cm^{-1} band decreases slightly on annealing to 8 K, while the others increase, and disappears on $\lambda > 380$ nm photolysis, while the others slightly increase. The 1828.6 cm^{-1} band gives a doublet mixed isotopic absorption for the vibration of a single carbonyl. Our BP86 calculation predicts the $RhCO^-$ absorption at 1843.6 cm^{-1} with unique large 1.0268 and small 1.0186 isotopic $^{12}CO/^{13}CO$ and $C^{16}O/C^{18}O$ frequency ratios, which are in excellent agreement with the observed 1.0257 and 1.0195 ratios, and confirms assignment of the 1828.6 cm^{-1} band to $RhCO^-$. This large $^{12}CO/^{13}CO$ and small $C^{16}O/C^{18}O$ isotopic ratio for a C−O stretching mode is due to the antisymmetric nature of C vibrating between Rh and O, the Rh−C bond strength, and the coupling of Rh−C and C−O vibrations.

The sharp 1814.4 cm^{-1} absorption and an associated 1900.4 cm^{-1} feature increase together on 8 K annealing and then decrease 5% on $\lambda > 290$ nm photolysis while the remaining 1864.8 and 1906.4 cm^{-1} bands slightly increase. The mixed ^{12}CO, ^{13}CO spectrum reveals triplet patterns and two equivalent carbonyls for the 1814.4 and 1900.4 cm^{-1} absorptions and suggests the $Rh(CO)_2^-$ assignment. Our BP86 calculation predicts 1813.2 cm^{-1} (b_2) and 1879.6 cm^{-1} (a_1) modes with 4.5/1 relative intensity, and isotopic frequency ratios which are in excellent agreement with the observed spectrum (Table 3). This agreement for two modes substantiates the $Rh(CO)_2^-$ assignment.

The 1864.8 cm^{-1} band is 80% destroyed on full-arc photolysis. The isotopic shifts denote a carbonyl motion and the four-band mixed isotopic pattern is characteristic of the doubly

(43) Bytheway, I.; Wong, M. W. *Chem. Phys. Lett.* **1998**, *282*, 219.

(44) Zhou, M. F.; Andrews, L. *J. Phys. Chem. A*, in press. (Co, Rh, Ir + CO).

Table 3. Bond Lengths, Isotopic C−O Stretching Frequencies (cm^{-1}), Intensities (km/mol), and Isotopic Frequency Ratios Calculated for Rhodium Dicarbonyl States

molecule	BL(Å)[a], BA(deg)	$(^{12}C^{16}O)_2$	$(^{13}C^{16}O)_2$	$(^{12}C^{18}O)_2$	*R*(12/13)	*R*(16/18)
$Rh(CO)_2^+$	1.964, 1.152, 104.4	2095.1(548) (b_2)	2047.7	2045.6	1.0231	1.0242
($^3B_2$)[b]		2124.8(118) (a_1)	2075.9	2075.8	1.0236	1.0236
$Rh(CO)_2^+$	2.009, 1.147, 180	2132.7(646) (σ_u)	2084.8	2081.8	1.0230	1.0244
($^3\Delta_g$)[b]		2180.2(0) (σ_g)	2129.2	2131.1	1.0240	1.0230
$Rh(CO)_2$	1.860, 1.176, 100.3	1946.8(997) (b_2)	1901.4	1902.9	1.0239	1.0231
($^2B_2$)[b]		2000.8(318) (a_1)	1953.0	1957.4	1.0245	1.0222
$Rh(CO)_2$	1.913, 1.172, 145.1	1961.4(1423) (b_2)	1916.8	1915.5	1.0233	1.0240
($^2A_1$)[b]		2027.8(104) (a_1)	1979.3	1983.7	1.0245	1.0222
$Rh(CO)_2$	1.931, 1.167, 180°	1974.0(1847) (σ_u)	1929.7	1926.8	1.0230	1.0245
($^2\Sigma_g^+$)[b]		2069.6(0) (σ_g)	2019.8	2025.2	1.0247	1.0219
$Rh(CO)_2$	1.946, 1.164, 180°	2004.1(1810) (σ_u)	1958.8	1956.9	1.0231	1.0241
($^2\Delta_g$)[b]		2086.8(0) (σ_g)	2036.7	2041.8	1.0246	1.0220
$Rh(CO)_2^-$	1.851, 1.201, 126.3°	1813.2(1671) (b_2)	1770.1	1773.7	1.0243	1.0223
($^1A_1$)[b]		1879.6(374) (a_1)	1833.1	1841.1	1.0254	1.0209

[a] Rh−C, C−O. [b] Relative energies (kcal/mol): $^2B_2$ (0.0), $^2A_1$ (2.4), $^2\Sigma_g^+$ (+4.2), $^2\Delta_g$ (+5.6), $^1A_1$ (−55.7), $^3\Delta_g$ (+199.9), $^3B_2$ (+202.4).

Scheme 1

+0.88 +0.05 +0.07	+0.12 -0.02 -0.10	-0.73 -0.04 -0.23
$RhCO^+$	RhCO	$RhCO^-$
ν_{CO} = 2174 cm^{-1}	ν_{CO} = 2022 cm^{-1}	ν_{CO} = 1828 cm^{-1}

degenerate (e) vibration of a trigonal species,[33−35,45] which is predicted at 1848.3 cm^{-1} at the BP86 level of theory.[44] Accordingly, the 1864.8 cm^{-1} band is assigned to $Rh(CO)_3^-$. The remaining 1906.4 cm^{-1} feature is 65% destroyed by full-arc photolysis. The five-band mixed isotopic spectrum is characteristic of the triply degenerate (t_2) vibration of a tetrahedral species,[33−35,45] which is calculated for tetrahedral $Rh(CO)_4^-$ at 1882.7 cm^{-1} using the BP86 functional.[44] This assignment is in agreement with the observation of $Rh(CO)_4^-$ in THF solution at 1900 cm^{-1}.[46] The $Rh(CO)_x^-$ anion absorptions are fit by our BP86 calculations with scale factors ranging from 0.992 to 1.013.

The 2184.7, 2174.1, and 2167.8 cm^{-1} bands are assigned to the $Rh(CO)_x^+$ cations. These bands along with CO^+ (2194.3 cm^{-1}) were enhanced on doping with CCl_4 to capture electrons that might otherwise neutralize cations, which supports the cation identification.[27,30,33−35] Annealing to 8 K with CCl_4 present *markedly* increased the 2167.8 cm^{-1} band. These bands all show carbonyl isotopic ratios but band congestion precludes observation of mixed isotopic counterparts so the order of band evolution with increasing CO concentration and on annealing provides the experimental evidence for *x* values. The 2174.1 cm^{-1} band is assigned to $RhCO^+$, the 2184.7 cm^{-1} absorption to $Rh(CO)_2^+$, and the 2167.8 cm^{-1} band to $Rh(CO)_3^+$. These assignments are strongly supported by BP86 frequency calculations, which predict strong C−O modes at 2129.4, 2132.7, and 2114.8 cm^{-1} (Tables 2, 3, ref 44). Our BP86 calculations find $^3\Delta$ and $^3\Delta_g$ ground states for $RhCO^+$ and $Rh(CO)_2^+$, in agreement with higher level calculations.[23] The BP86 frequency calculations for $Rh(CO)_{1,2,3}^+$ are 1−2% lower than observed for the isolated cations in solid neon.

Comparisons with Rhodium Carbonyl Surface Species. The carbonyl frequencies of $RhCO^+$ (2174 cm^{-1}), RhCO (2022 cm^{-1}), and $RhCO^-$ (1828 cm^{-1}) show a pronounced dependence on net charge. The calculated Mulliken charges show that most of the net charge resides on the metal (Scheme 1). An added electron decreases the Rh−C bond length and increases the C−O bond length, thus decreasing the C−O frequency (Table 2). Hence, the carbonyl stretching frequency is a measure of charge on the RhCO species, which approximates local charge on the Rh metal center. In the case of CO bonded to cation centers, these so-called "non-classical" carbonyls with frequencies higher than CO itself have been explained by electrostatic effects[47] and have also been observed in zeolites for alkali cations.[48] We offer the $RhCO^+$, RhCO, and $RhCO^-$ frequencies as a scale for estimating charge on Rh in the active catalyst media and plot our observed monocarbonyl frequency vs net charge in Figure 2. The observed points are connected by straight lines without implying a functional form; however, the $RhCO^+$ matrix shift is probably 2 to 3 times that of RhCO and $RhCO^-$ so that a gas phase plot would be approximately linear. The highest frequency for $Na^q(CO)$/zeolite at 2178 cm^{-1} almost matches our isolated $RhCO^+$ at 2174 cm^{-1} so $q = +1.0$ is a reasonable description of local charge. The frequency for Rh^q-

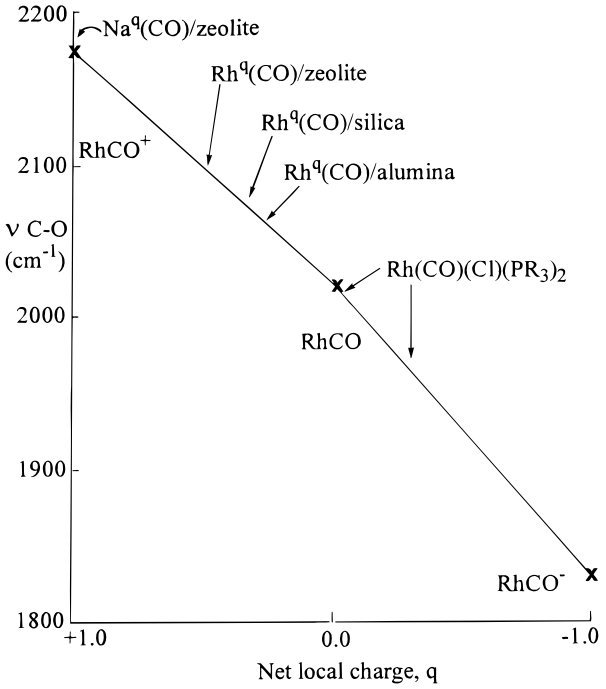

Figure 2. Plot of $RhCO^+$, RhCO, and $RhCO^-$ carbonyl stretching frequencies observed in solid neon vs net local charge on each RhCO species.

(45) Darling, J. H.; Ogden, J. S. *J. Chem. Soc., Dalton Trans.* **1972**, 2496.

(46) Chini, P.; Martinengo, S. *Inorg. Chim. Acta* **1969**, *3*, 21.

(47) Goldman, A. S.; Krogh-Jespersen, K. *J. Am. Chem. Soc.* **1996**, *118*, 12159.

(48) Zecchina, A.; Areán, C. O. *Chem. Soc. Rev.* **1996**, *25*, 187.

(49) Wang, H. P.; Yates, J. T., Jr. *J. Catal.* **1984**, *89*, 79.

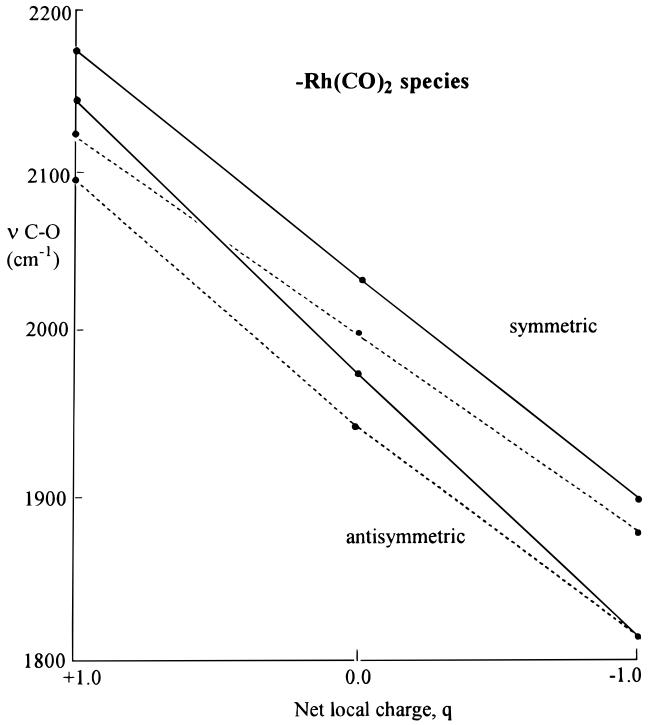

Figure 3. Plots of symmetric and antisymmetric carbonyl stretching frequencies calculated (BP86/D95*/ECP) for low-lying bent states of $Rh(CO)_2^+$, $Rh(CO)_2$, and $Rh(CO)_2^-$ (dashed lines) and the same frequencies scaled (bold lines) by neon matrix frequencies observed for linear $Rh(CO)_2^+$ and $Rh(CO)_2$ and bent $Rh(CO)_2^-$ vs net local charge on each species.

(CO)/zeolite at 2096 cm^{-1} is halfway between $RhCO^+$ and RhCO and q near +0.5 is proposed. The $Rh^q(CO)$/alumina frequency at 2060 cm^{-1} suggests q near +0.3. The Rh(CO)-(Cl)$(PR_3)_2$ complexes range from $q = 0$ to −0.3 and the CpRh-(CO) transient at 1985 cm^{-1} indicates a slightly negative charge near −0.2.

Correlation of infrared spectra with charge in the important gem−rhodium dicarbonyl $Rh^q(CO)_2$ is more complicated because the isolated $Rh(CO)_2$ and $Rh(CO)_2^+$ benchmarks observed here are linear and the gem surface species is bent with comparable intensities for symmetric and antisymmetric C−O vibrations. However, our DFT calculations model antisymmetric carbonyl stretching modes for the isolated linear $Rh(CO)_2^+$ cation and linear $Rh(CO)_2$ radical frequencies 2.4 and 1.3% low and the bent $Rh(CO)_2^-$ species only 0.1% low, so that we conclude that similar DFT calculations for bent $Rh(CO)_2^+$ and $Rh(CO)_2$ states should be equally accurate. Our calculations for the bent ($^3B_2$, 104°) $Rh(CO)_2^+$ cation predict symmetric and antisymmetric C−O frequencies of 2125 and 2095 cm^{-1}, respectively, and for bent ($^2B_2$, 100°) $Rh(CO)_2$ predict 2001 and 1947 cm^{-1}. These are plotted as dashed lines in Figure 3 along with the 1880 and 1813 cm^{-1} frequencies calculated for $Rh(CO)_2^-$ ($^1A_1$, 126°) against the net local charge, q. Next, the calculated frequencies for bent $Rh(CO)_2^+$ and bent $Rh(CO)_2$ are scaled by factors determined from our calculated and observed frequencies for the linear $Rh(CO)_2^+$ and $Rh(CO)_2$, species and plotted with the neon matrix frequencies for $Rh(CO)_2^-$ as solid lines in Figure 3. Now, if the observed symmetric and antisymmetric 2100 and 2030 cm^{-1} frequencies for $Rh^q(CO)_2$ on alumina[1−9] are fit to the solid scaled curves for bent $Rh^q(CO)_2$ species, charges of +0.5 and +0.3 are predicted. We estimate that the net local charge, q, on the Rh^q-$(CO)_2$ species on alumina is approximately +0.4 using scaled calculated frequencies for bent dicarbonyl species. Likewise for $Rh^q(CO)_2$ on zeolite,[16] the higher 2118 and 2053 cm^{-1} frequencies indicate a higher positive charge near +0.5. The charge q is clearly less than +1 but more than 0 for these supported dicarbonyl species.

Clearly charge is more delocalized in $Rh(CO)_2$ than in RhCO. Mulliken charge distributions calculated for linear $^2\Delta_g$ $Rh(CO)_2$ are Rh (+0.23), C (−0.06), O (−0.05) and for bent $^2B_2$ Rh-$(CO)_2$ are Rh (+0.24), C (−0.04), O (−0.08). As a consequence, note that carbonyl frequencies are calculated 60−90 cm^{-1} *lower* for the $^2B_2$ bent $Rh(CO)_2$ species (Table 3). Higher level calculations find $^3\Delta$ $RhCO^+$ with Rh (+0.77), just less than our result, and linear $^3\Delta_g$ $Rh(CO)_2^+$ has Rh (+0.55).[23] The carbonyl frequencies discussed here are a consequence of net local charge on the entire rhodium carbonyl species, which includes the carbonyl moiety and the metal center.

At high CO pressures, the $Rh^q(CO)_2$ species on alumina is converted to a $Rh^q(CO)_3$ moiety characterized as distorted from the observation of three infrared bands 2120 cm^{-1} (weak), 2078 cm^{-1} (very strong), and 2026 cm^{-1} (strong).[49] Our BP86 calculations for $Rh(CO)_3^+$ and $Rh(CO)_3$ predict distorted "T-shaped" species with strong antisymmetric frequencies 2.4 and 1.9% below the neon matrix values.[44] The very strong 2078 cm^{-1} band for the surface species corresponds to the antisymmetric mode, and this band is 40% of the way between our neon matrix observations for $Rh(CO)_3$ (2020 cm^{-1}) and Rh-$(CO)_3^+$ (2168 cm^{-1}). From this observed tricarbonyl scale, we conclude that $q = +0.4$. Our frequency correlation estimates of q for the $Rh^q(CO)_{1,2,3}$ species on alumina are remarkably consistent (q values +0.3, 0.4, 0.4, respectively).

Conclusions

In summary, laser-ablated Rh^+, Rh and electrons react with CO on condensation in excess neon to form $RhCO^+$, RhCO, $RhCO^-$ and $Rh(CO)_2^+$, $Rh(CO)_2$, $Rh(CO)_2^-$ (and higher carbonyls which will be described fully in a later paper[44]). These rhodium carbonyls are identified by isotopic substitution, electron trapping with added CCl_4, and comparison with DFT structure and frequency calculations. Our BP86/D95*/ECP calculations predict the carbonyl stretching frequencies within 1−2% of the neon matrix values. Finally, the isolated neon matrix monocarbonyl cation, neutral, and anion frequencies provide a scale to estimate net charge on Rh(CO) species in active catalyst systems using the observed carbonyl stretching frequency.

Acknowledgment. We gratefully acknowledge NSF support under Grant CHE 97-00116 and helpful discussions with H. Frei, I. Harrison, and W. D. Harman.

JA991180J